AGU PUBLICATIONS

Geophysical Research Letters

RESEARCH LETTER
10.1002/2015GL067490

Key Points:
- Dynamic friction weakening scales as a power law of slip
- The generalized weakening form explains the observed scaling of earthquake fracture energy
- In large earthquakes, dominating dissipation is not friction but rather plastic, off-fault strain

Supporting Information:
- Supporting Information S1
- Data Set S1
- Data Set S2

Correspondence to:
S. Nielsen,
stefan.nielsen@durham.ac.uk

Citation:
Nielsen, S., E. Spagnuolo, S. A. F. Smith, M. Violay, G. Di Toro, and A. Bistacchi (2016), Scaling in natural and laboratory earthquakes, *Geophys. Res. Lett.*, *43*, 1504–1510, doi:10.1002/2015GL067490.

Received 19 DEC 2015
Accepted 29 JAN 2016
Accepted article online 1 FEB 2016
Published online 20 FEB 2016

Scaling in natural and laboratory earthquakes

S. Nielsen[1,2], E. Spagnuolo[1], S. A. F. Smith[1,3], M. Violay[1,4], G. Di Toro[1,5], and A. Bistacchi[6]

[1]Istituto Nazionale di Geofisica e Vucanologia, Rome, Italy, [2]Now at Earth Sciences Department, Durham University, Durham, United Kingdom, [3]Now at Department of Geology, University of Otago, Dunedin, New Zealand, [4]Now at EPFL, Lausanne, Switzerland, [5]Now at School of Earth, Atmospheric and Environmental Sciences, University of Manchester, Manchester, United Kingdom, [6]DISAT, Universitá degli Studi Milano-Bicocca, Milan, Italy

Abstract Laboratory experiments reproducing seismic slip conditions show extreme frictional weakening due to the activation of lubrication processes. Due to a substantial variability in the details of the weakening transient, generalization of experimental results and comparison to seismic observations have not been possible so far. Here we show that during the weakening, shear stress τ is generally well matched by a power law of slip u in the form $\tau \propto u^{-\alpha}$ (with $0.35 < \alpha < 0.6$). The resulting fracture energy G_f can be approximated by a power law in some aspects in agreement with the seismological estimates G'. It appears that G_f and G' are comparable in the range $0.01 < u < 0.3$ m. However, G' surpasses G_f at larger slips: at $u \approx 10$ m, $G' \approx 10^8$ and $G_f \approx 10^6$. Possible interpretations of this misfit involve the complexity of damage and weakening mechanisms within mature fault zone structures.

1. Introduction

During earthquakes, shear stress is rapidly released because of a drop in friction, causing high slip velocity (≈1 m/s), high rupture propagation velocity (≈1 km/s) and wave radiation. Shear stress drops with slip and slip velocity, a process known as weakening. The simplest and most widely adopted model for frictional weakening [*Ida*, 1972] consists of a linear decrease of shear stress with slip from peak τ_p to steady state τ_{ss}, over a weakening distance D_c. It is recognized [*Palmer and Rice*, 1973] that frictional work (product of shear stress and slip) during the weakening process equates to a particular form G_f of fracture energy G, such that

$$G_f = \frac{1}{2}(\tau_p - \tau_{ss})\, D_c\,, \tag{1}$$

assuming linear slip weakening law [*Ida*, 1972], whereas the slightly more general form [*Abercrombie and Rice*, 2005]:

$$G_f(u) = \int_0^u \left(\tau(u') - \tau(u)\right) \mathrm{d}u'\,, \tag{2}$$

can take into account nonlinear friction decay and considers the possibility that the shear stress does not necessarily drop to the lowest possible dynamic value τ_{ss} (slip $u < D_c$) in all earthquakes.

Seismological estimates of D_c suffer from poor resolution and from a fundamental indetermination: rupture is mainly sensitive to G_f [*Peyrat et al.*, 2004], which is in essence the product of strength drop $(\tau_p - \tau_{ss})$ and D_c, as shown in equation (1), so that both cannot be determined independently, save for exceptional circumstances [*Cruz-Atienza and Olsen*, 2010].

Ultimately, fault properties which control rupture propagation are better represented by fracture energy rather than by specific aspects of the weakening process. In addition, G appears in the energy balance [*Abercrombie and Rice*, 2005] against radiated energy (which can be estimated from detected waves) and elastic strain release (which can be estimated from final fault slip). As a consequence, under a series of assumptions, it is possible to obtain G', a seismological estimate of G and its variation with seismic moment and slip, as proposed by several authors [*Aki*, 1979; *Abercrombie and Rice*, 2005; *Tinti et al.*, 2005; *Malagnini et al.*, 2013; *Viesca and Garagash*, 2015].

Here we analyze in detail the features of the experimental weakening curves, provide a general functional fit, and discuss the resulting fracture energy G_f (according to equation (2)) in relation to seismological estimates G'.

2. Anatomy of the Experimental Weakening Curves

We use a representative sample selected from a catalog of hundreds of experiments performed on the rotary Slow to HIgh Velocity Apparatus (SHIVA) installed at the HP-HT laboratories at INGV-Rome [*Di Toro et al.*, 2010]. The experiments are performed under conditions approaching those of earthquakes: normal stress in the range 5–40 MPa, slip velocity 1–6.5 m/s, and slip acceleration 3–6.5 m/s^2. Both solid, precut rock cylinders or layers of powdered rock gouge were used for experiments under atmospheric humidity conditions. A pressure vessel with water-permeated solid samples was used to investigate the role of pore pressure in the frictional weakening. Selected rocks are representative of seismic environments: silicate-bearing rocks (microgabbro [*Niemeijer et al.*, 2011], basalt [*Violay et al.*, 2014], Westerly granite, tonalite from fossil seismic faults [*Di Toro et al.*, 2006]), carbonate rocks (Carrara marble with 99% calcite [*Violay et al.*, 2015]), and natural seismic fault gouge [*Kuo et al.*, 2013] rich in clay and quartz minerals (experimental methods are described in detail in the references above).

In high-velocity friction experiments on dry gouge and on either dry or wet bare rock, the observed abrupt dynamic weakening has been attributed to thermal decomposition and phase changes triggered under intense frictional heating [*Han et al.*, 2007; *Di Toro et al.*, 2011], including localized flash heating and weakening [*Rice*, 2006; *Noda et al.*, 2009] of contact asperities. However, in clay-rich gouges, different processes were observed resulting in a slower and less significant dynamic weakening [*Kuo et al.*, 2013]. Experiments performed on solid rock samples immersed in water do also show evidence of thermal pressurization. However, in this case its role is minor because other thermal weakening mechanisms (melting or decomposition) intervene more rapidly and efficiently [*Violay et al.*, 2015]. Note that current experiments do not allow confinement of wet gouges: in such case we cannot exclude that thermal pressurization would dominate, producing weakening curves in agreement with models of *Rice* [2006] and *Viesca and Garagash* [2015].

Dynamic weakening observed during high-velocity friction experiments show substantial variations depending on mineralogy and loading conditions. However, when the experimental procedure is accurate enough to allow good signal-to-noise ratio and a high degree of repeatability [*Violay et al.*, 2015], several systematic features are observed.

As illustrated in Figure 1b, upon rapid loading, shear stress rises linearly with strain as the sample is elastically loaded prior to the start of slip (phase 0). A short slip (phase I) then occurs under high, almost constant or slightly strain-hardening friction (compatible with Byerlee's law with a friction coefficient >0.5). Phase I gives way very early (<1 cm of slip, which corresponds roughly to slip rates of the order of 16 cm/s under high imposed accelerations) to (phase II) when the high frictional power triggers efficient lubrication processes [*Di Toro et al.*, 2011], and thus abrupt weakening is initiated. During all of phase II, friction drops with slip following a linear trend in a log-log diagram (Figure 1b).

In the case of carbonate rocks an intermediate phase (IIb) is observed during which a slight weakening continues even after the end of slip acceleration; in such case phase III is reached only after several meters of slip. During phase IIb, friction versus slip still appears as log-log linear but with a reduced slope.

Deceleration of slip (phase IV) is characterized by a rapid recovery of friction; in many experiments the recovery reaches about 20% of the peak stress. This value depends on the imposed deceleration rate: friction response to velocity change is not instantaneous, so that a faster deceleration results in reduced recovery.

During the abrupt weakening phase, shear stress is best described by a power law of the form $\tau \propto u^{-\alpha}$ where $0.5 < \alpha < 0.6$ for phase II ($\alpha \approx 0.35$ for phase IIb). Given that the weakening phase is tapered at its beginning by an approximately constant, peak value τ_p and at its end by the steady state, dynamic sliding value τ_{ss}, the three different branches can be described by:

$$u \ll u_w, \quad \tau \approx \tau_p \tag{3}$$

$$u_w < u < u_w(\tau_p/\tau_{ss} - 1)^{1/\alpha}, \quad \tau \approx \tau_p \left(\frac{u}{u_w}\right)^{-\alpha} \tag{4}$$

$$u \gg u_w(\tau_p/\tau_{ss} - 1)^{1/\alpha}, \quad \tau \approx \tau_{ss} \tag{5}$$

where u_w is the slip value at which weakening is initiated; τ will have dropped to steady state value τ_{ss} when slip has reached $u = u_w(\tau_p/\tau_{ss} - 1)^{1/\alpha}$. The fit corresponding to equations (3)–(5) and combined function in the supporting information) is represented as a dashed curve along with the experimental data in Figure 1.

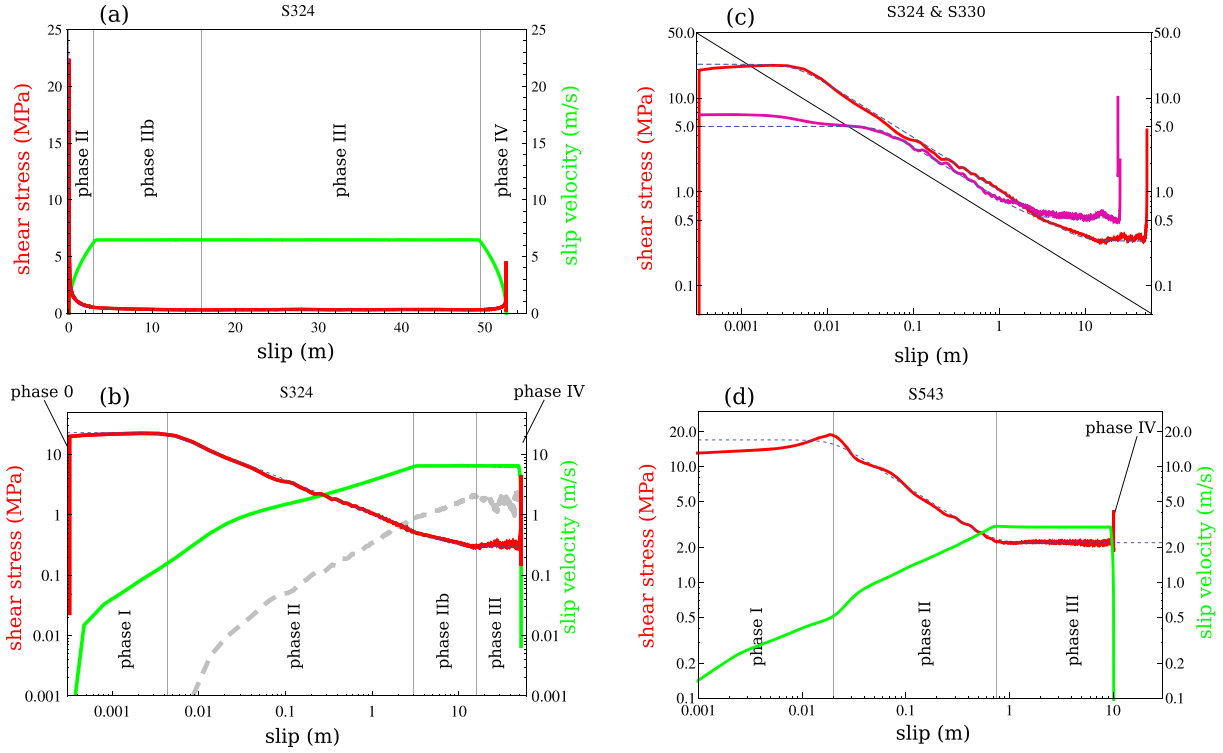

Figure 1. (a) Experiment S234, performed on calcite (Carrara marble) at normal stress 30 MPa, slip acceleration 6.5 m/s^2, and target slip velocity 6.5 m/s. Linear plot of slip versus slip velocity (green), shear stress (red) and its power law fit according to equation (4) (dashed) against slip, with parameters $u_w = 0.0043$ m, $\tau_p = 23$ MPa, $\tau_{ss} = 0.3$ MPa, $\alpha = 0.57$. (b) Same as Figure 1a plotted in log-log scale. G_f is indicated as a grey dashed curve. (c) Comparison of log shear stress against log slip for experiments S324 (red) and S330 (purple), performed on carbonate rock (Carrara marble). For S330, maximum slip velocity and normal stress are 3 m/s and 10 MPa, respectively; fit (dashed curves) is with parameters $u_w = 0.045$ m, $\tau_p = 5$ MPa, $\tau_{ss} = 0.53$ MPa, $\alpha = 0.57$. (d) Experiment S543, performed on silica-bearing rock (microgabbro) at normal stress 30 MPa, slip acceleration 6.5 m/s^2, and target slip velocity 6.5 m/s. Log-log plot of slip versus slip velocity (green), shear stress (red), and its power law fit with parameters $u_w = 0.02$ m, $\tau_p = 17$ MPa, $\tau_{ss} = 2.2$ MPa, $\alpha = 0.57$. Here no phase IIb is observed: as soon as the slip velocity becomes constant, the steady state is reached.

The experiments start with a brief (0.5–1 s) velocity ramp of constant slip acceleration ($\dot{V} = 6.5$ m/s^2 in most experiments). During the acceleration phase then $t = V/\dot{V}$ and slip $u = \frac{1}{2}\dot{V}t^2$, which yield velocity $V \approx \sqrt{2\,u\,\dot{V}}$. Assuming that weakening is triggered once a critical slip velocity V_w has been reached, then the corresponding slip is

$$u_w \approx \frac{1}{2}\frac{V_w^2}{\dot{V}}. \tag{6}$$

For experiment S324 (Figures 1a and 1b) we measure $V_w \approx 0.16$ m/s and $\dot{V} \approx 3$ m s^{-2}, resulting in $u_w \approx 0.0043$ m. In phase II the best fit value for the exponent is $\alpha = 0.57$. This value holds for quite different experiments; a comparison of two experiments performed on carbonate rock under different maximum slip velocity and normal stress shows that phase II is very similar (Figure 1c). The change in the loading conditions mainly affects the values of τ_p, τ_{ss} and u_w. Using the rough approximation that $\tau \propto 1/V$ during the weakening phase and noting that $V = \sqrt{2\,u\,\dot{V}}$ under constant acceleration, one would obtain $\tau \propto \frac{1}{\sqrt{2\,\dot{V}}}u^{-0.5}$, where 0.5 is fairly close to the experimental fit of 0.57. Thus, in the first approximation high-velocity friction shows inverse velocity weakening, in agreement with models invoked to explain the spontaneous formation of seismic pulses in earthquakes [*Cochard and Madariaga*, 1994, and references therein].

In the case of silicate-bearing rocks no phase IIb is observed; steady state (phase III) is achieved almost immediately after the target slip velocity has been reached (end of acceleration phase), where a low sliding friction value (<0.1) is maintained, with minor fluctuations, as long as slip rate is not modified. (Note that in experiments under lower normal stress on gabbro, the steady state is achieved much later and a second peak of strengthening is observed [*Hirose and Shimamoto*, 2005]. In the experiments discussed here, weakening is accelerated due to the larger frictional power dissipated and no second peak is observed [*Nielsen et al.*, 2010; *Di Toro et al.*, 2011]). Contrary to carbonate rocks, frictional melt and extrusion of melt out of the slipping

zone takes place in silicate-rich rocks with relatively rapid shortening of the sample [*Nielsen et al.*, 2008, 2010] (shortening rate $v \approx 1$ mm/s or more under experimental conditions described here). The sample shortening catches up with the thermal diffusion, creating a thermal boundary layer of finite thickness in such a way that a steady state is rapidly reached. With increased frictional power dissipation (hence with increased slip velocity, acceleration, and normal stress), sample shortening velocity v is faster and steady state is achieved in reduced time and slip amounts. One example for gabbro (experiment S543) is shown in Figure 1d. The main differences as compared to the calcite experiment of Figure 1b are a slight slip-hardening (phase I) before weakening and the absence of phase IIb. Besides these differences, the same general fit (4) and exponent as for the calcite example applies to cases of frictional melting.

For experiments performed in gouge, weakening is preceded by a marked strain-hardening phase [*Smith et al.*, 2015] but is otherwise as described above.

3. Fracture Energy G_f

Using equations (3) and (4) we can obtain a theoretical fracture energy

$$G_f(u) = u_w \tau_p \left(\frac{\alpha}{\alpha - 1} + \left(\frac{u}{u_w} \right)^{-\alpha} + \frac{1}{1-\alpha} \left(\frac{u}{u_w} \right)^{1-\alpha} \right) \tag{7}$$

by integrating the frictional weakening according to equation (2). Given that $\alpha < 1$, in the case that $u \gg u_w$ we may neglect the first two terms to obtain

$$\begin{aligned} G_f(u) &\approx \frac{1}{1-\alpha} u_w \tau_p \left(\frac{u}{u_w} \right)^{1-\alpha} \quad \text{for} \quad u < u_w (\tau_p / \tau_{ss} - 1)^{1/\alpha}, \\ G_f(u) = \text{const.} &\approx \frac{1}{1-\alpha} u_w \tau_p \left(\tau_p / \tau_{ss} - 1 \right)^{\frac{1-\alpha}{\alpha}} \quad \text{for} \quad u \geq u_w (\tau_p / \tau_{ss} - 1)^{1/\alpha}. \end{aligned} \tag{8}$$

the second equation indicates that G_f saturates after reaching the steady state with τ_{ss} at $u = u_w(\tau_p/\tau_{ss} - 1)^{1/\alpha}$. Measures of a slip-weakening distance D_c have been attempted previously in high-velocity friction experiments [*Hirose and Shimamoto*, 2005; *Nielsen et al.*, 2008, 2010], assuming an exponential decay. However, considering the weakening part of the curves as a power law tapered by initial (τ_p) and steady state (τ_{ss}) values, the weakening distance D_c may require a redefinition based on the saturation distance $u = u_w(\tau_p/\tau_{ss} - 1)^{1/\alpha}$.

Using τ and u measured in the experiments, the discrete equivalent of equation (2) allows to obtain an experimental curve $G_f(u)$. (Friction recovery during the deceleration takes place within a very small slip amount, so that the frictional energy related to recovery is negligible in the computation of G_f.) An example of the resulting $G_f(u)$ curve is shown in Figure 1b for a single experiment. For 28 experiments performed on a variety of lithologies and conditions, the average G_f values are shown in Figure 2 in red (vertical bars indicate standard deviation between the experiments). Although scatter is present at small slip amounts, a general trend common to all experiments is clear. (G_f curves corresponding to individual experiments are found in the supporting information.)

The scaling of G_f in equation (1) and Figure 2 show features (log-linear increase with slip) which qualitatively agree with independent estimates [*Abercrombie and Rice*, 2005] of earthquake fracture energy G' from a number of earthquake data:

$$G' = 5.25\ 10^6\ u^{1.28} \tag{9}$$

and also with the slightly more complex scaling from a more recent compilation [*Viesca and Garagash*, 2015]. We recall that G' estimates assume no undershoot or overshoot in earthquakes: this may introduce bias [*Abercrombie and Rice*, 2005] up to 1 order of magnitude [*Viesca and Garagash*, 2015] in fracture energy. In addition, G' estimates represent average measures for a highly inhomogeneous process. Mega-earthquakes ($u \geq 10$ m) radiate very low frequencies at which radiated energy—and G' as a consequence—are difficult to measure. As a consequence, a large variability is expected in estimates of G', as observed in Figure 2. Due to the inclusion of dynamic numerical simulations results (tcss) producing systematic higher G' values, variability here is perceptibly larger than in [*Viesca and Garagash*, 2015].

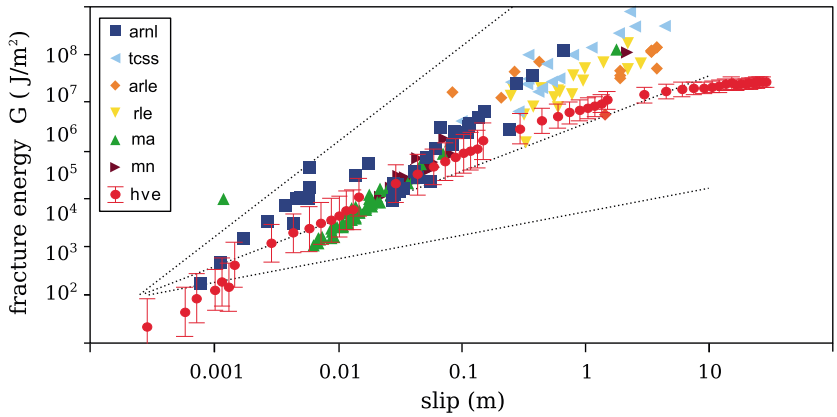

Figure 2. Laboratory (G_f, in red) and seismological (G', other colors) estimates of fracture energy under coseismic slip conditions. Red disks correspond to the average G_f for 28 high-velocity experiments (hve, this study), shown at various slip amounts; the standard deviations (vertical bars) indicate the scatter due to the variety of lithologies and experimental conditions. Squares, triangles, and diamonds correspond to seismological estimates G'. arnl: Northridge aftershocks [*Abercrombie and Rice*, 2005]; arle :large earthquakes [*Abercrombie and Rice*, 2005]; tcss: numerical simulations [*Tinti et al.*, 2005]; rle: large earthquakes [*Rice*, 2006]; ma: L'Aquila [*Malagnini et al.*, 2013]; mn: Northridge sequence [*Malagnini et al.*, 2013]. Dashed lines indicate exponent 0.5, 1, and 2 for reference.

As shown in Figure 2, G_f and G' are comparable; both increase with slip within the range $0.001 < u < 0.3$ m (approximate magnitudes $1 < M_w < 6$ and $10^4 < G < 10^6$ J m^{-2}). However, G' becomes perceptibly larger than G_f in the range of slip $u > 0.3$ m, and the overall exponent in G_f ($1 - \alpha \approx 0.4 - 0.65$) is lower than that in G' ($1 - \alpha \approx 1.28$). For large slips ($u \approx 10$ m) the difference reaches 2 orders of magnitude ($G' \approx 10^8$ and $G_f \approx 10^6$ J/m^2). We discuss below several possible interpretations of such discrepancy.

4. Discussion

Assuming that $G'(u)$ and shear stress $\tau(u)$ are related through equation (2), the derivative of (9) with respect to u results, after some algebra [*Abercrombie and Rice*, 2005], in a stress evolution of the following form:

$$\tau(u) = \tau_p - 4.8\,10^6\,u^{0.28}. \tag{10}$$

If this form were used with very low values of τ_p (e.g., 5 MPa) and relatively high values of u (e.g., 10 m), it may result in the unphysical feature of a negative friction. A value greater than 1 in the exponent in equation (9) produces an unphysical situation if we assume that G' is related to frictional dissipation along the fault surface alone. As noted elsewhere [*Shipton et al.*, 2006] the effective G' observed at the seismological scale should implicitly incorporate energy sinks other than friction.

Normal stress influences τ_p, τ_{ss}, and weakening distance; hence, it could also affect fracture energy, producing a discrepancy between experimental and natural G. However, previous theoretical modeling [*Nielsen et al.*, 2010] and experimental data regarding frictional melt predicted no systematic variation of fracture energy with normal stress. Here we confirm and extend this result to a wider range of normal stress and to cases where either frictional melt takes place (gabbro, basalt) or not (carbonate). Figure 3 shows a collection of fracture energies measured under different normal stress and at three different values of slip. No systematic trend is observed in G_f as normal stress varies from 10 to 40 MPa.

The samples used here closely replicate the structures observed on small to intermediate ($M_w \approx 2$–6) earthquake faults [*Di Toro et al.*, 2006]. However, mature faults hosting larger earthquakes develop a damage zone structure far more complex and wide than in the experimental samples. Though analysis of cores indicate that slip is localized on a very thin (<100 μm) principal slip zone, it is likely that the surrounding fault zone alters the mechanical behavior during rupture in nontrivial ways. In particular, for favorable combinations of hydrothermal diffusivity and width of the actively shearing gouge, thermal pressurization can result in gradual weakening in agreement with the seismological estimates of G [*Viesca and Garagash*, 2015].

The roughness of natural faults [*Bistacchi et al.*, 2011; *Candela et al.*, 2012] creates additional stress [*Griffith et al.*, 2010] and strain during slip, resulting in frictional drag [*Dunham et al.*, 2011] which increases with slip,

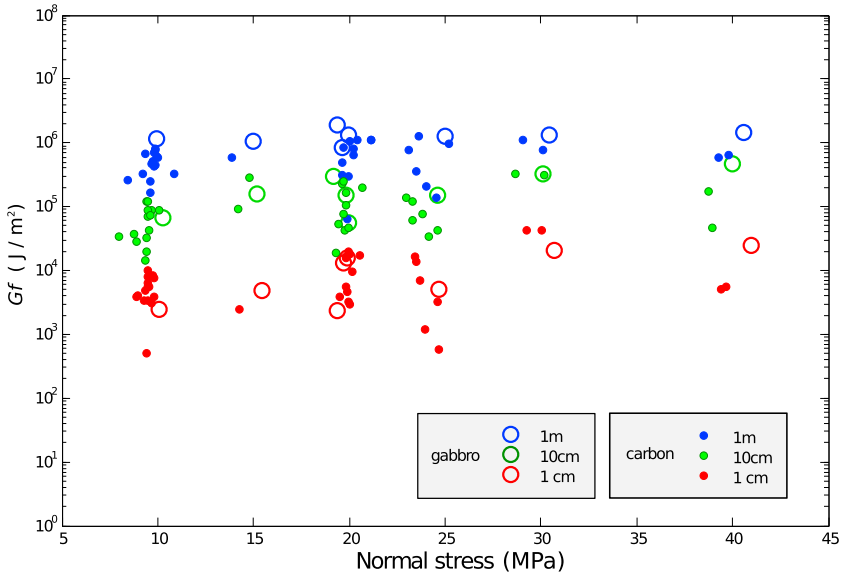

Figure 3. Measure of fracture energy for experiments performed under different normal stress (in the range 10 to 40 MPa) and three different slip amounts (red = 1 cm, green = 10 cm, blue = 1 m). No significant trend is observed with normal stress. The increase with slip replicates the observation of Figures 1 and 2. (Open circles represent gabbro experiments; colored disks represent experiments on carbonate rock.) No significant dependance of G_f on normal stress is observed.

introducing work in addition to friction. Roughness also result in asperity abrasion (especially at small wavelengths) and off-fault damage which will introduce additional energy sinks. Even on a planar fault, off-fault stress associated to rupture propagation is sufficiently high to induce anelastic damage in a band of finite thickness, with dissipation per unit fault area increasing proportionally to fault length [*Poliakov*, 2002; *Andrews*, 2005]. In earthquake scaling, slip is proportional to fault length [*Aki*, 1979], so that fracture energy resulting from such off-fault dissipation would scale as $G' \propto u^{1.0}$. Exponents 1.0 and 1.28 are possibly compatible, within the precision of seismological estimates. This scaling is also compatible with the barrier toughness model for the arrest of crack growth [*Aki*, 1979]. Hence, plastic strain associated to the stress concentration at the tip of the propagating rupture may account for the scaling of G'.

Rapid and efficient lubrication is triggered upon frictional sliding in high-velocity experiments on dry gouges and in dry and wet rocks. The resulting fracture energy is compatible with that estimated from small to intermediate earthquake (M_w 2–6). However, experiments underpredict fracture energy of large earthquakes. One possible intepretation is that other dissipative forms than friction dominate in large earthquakes: diffusive processes such as thermal pressurization in the wider damage zone and plastic, off-fault strain resulting from fault roughness and from stress concentrations around the fracture tip.

Acknowledgments
We thank N. Brantut and R. Madariaga for insightful reviews. We acknowledge funding by the European Research Council projects 205175 (USEMS) and 614705 (NOFEAR). S.N. acknowledges support from NERC capital grant CC019 (HiFAST). S.A.F.S. acknowledges funding from the Marsden Fund Council (project UOO1417 to Smith), administered by the Royal Society of New Zealand S.N., E.S., M.V., S.A.F.S, and G.D.T. contributed to the realization of the experiments. All authors contributed in developing the main ideas, interpreting the results, and producing the manuscript. Supporting information is available in the online version of the paper. Correspondence and requests for materials should be addressed to S.N. or E.S. All authors declare no conflict of interests.

References

Abercrombie, R., and J. Rice (2005), Can observations of earthquake scaling constrain slip weakening?, *Geophys. J. Int.*, *162*, 406–424.
Aki, K. (1979), Characterization of barriers on an earthquake fault, *J. Geophys. Res.*, *84*, 6140–6148.
Andrews, D. J. (2005), Rupture dynamics with energy loss outside the slip zone, *J. Geophys. Res.*, *110*, B01307, doi:10.1029/2004JB003191.
Bistacchi, A., W. Griffith, S. Smith, G. Di Toro, R. Jones, and S. Nielsen (2011), Fault roughness at seismogenic depths from LIDAR and photogrammetric analysis, *Pure Appl. Geophys.*, *168*, 2345–2363.
Candela, T., F. Renard, Y. Klinger, K. Mair, J. Schmittbuhl, and E. E. Brodsky (2012), Roughness of fault surfaces over nine decades of length scales, *J. Geophys. Res.*, *117*, B08409, doi:10.1029/2011JB009041.
Cochard, A., and R. Madariaga (1994), Dynamic faulting under rate-dependent friction, *Pure Appl. Geophys.*, *142*, 419–445.
Cruz-Atienza, V., and K. Olsen (2010), Supershear Mach-waves expose the fault breakdown slip, *Tectonophysics*, *493*, 285–296, doi:10.1016/j.tecto.2010.05.012.
Di Toro, G., T. Hirose, S. Nielsen, G. Pennacchioni, and T. Shimamoto (2006), Natural and experimental evidence of melt lubrication of faults during earthquakes, *Science*, *311*, 647–649, doi:10.1126/science.1121012.
Di Toro, G., et al. (2010), From field geology to earthquake simulation: A new state-of-the-art tool to investigate rock friction during the seismic cycle (shiva), *Rendiconti Lincei*, *21*, 95–114, doi:10.1007/s12210-010-0097-x.
Di Toro, G., R. Han, T. Hirose, N. De Paola, S. Nielsen, K. Mizoguchi, F. Ferri, M. Cocco, and T. Shimamoto (2011), Fault lubrication during earthquakes, *Nature*, *471*, 494–499, doi:10.1038/nature09838.

Dunham, E. M., D. Belanger, L. Cong, and J. E. Kozdon (2011), Earthquake ruptures with strongly rate-weakening friction and off-fault plasticity, Part 2: Nonplanar faults, *Bull. Seismol. Soc. Am.*, *101*(5), 2308–2322, doi:10.1785/0120100076.

Griffith, W. A., S. Nielsen, G. Di Toro, and F. A. S. Smith (2010), Rough faults, distributed weakening, and off-fault deformation, *J. Geophys. Res.*, *115*, B08409, doi:10.1029/2009JB006925.

Han, R., T. Shimamoto, T. Hirose, J.-H. Ree, and J. Ando (2007), Ultralow friction of carbonate faults caused by thermal decomposition, *Science*, *316*, 878–881, doi:10.1126/science.1139763.

Hirose, T., and T. Shimamoto (2005), Growth of molten zone as a mechanicsm of slip weakening of simulated faults in gabbro during frictional melting, *J. Geophys. Res.*, *110*, B05202, doi:10.1029/2004JB003207.

Ida, Y. (1972), Cohesive force across the tip of a longitudinal-shear crack and Griffith's specific surface energy, *J. Geophys. Res.*, *77*, 3796–3805.

Kuo, L.-W., H. Li, S. A. F. Smith, G. Di Toro, J. Suppe, S.-R. Song, S. Nielsen, H.-S. Sheu, and J. Si (2013), Gouge graphitization and dynamic fault weakening during the 2008 M_W 7.9 Wenchuan earthquake, *Geology*, *42*(1), 47–50, doi:10.1130/g34862.1.

Malagnini, L., I. Munafò, M. Cocco, S. Nielsen, K. Mayeda, and E. Boschi (2013), Gradual fault weakening with seismic slip: Inferences from the seismic sequences of L'Aquila, 2009, and Northridge, 1994, *Pure Appl. Geophys.*, *171*(10), 2709–2730, doi:10.1007/s00024-013-0752-0.

Nielsen, S., G. Di Toro, T. Hirose, and T. Shimamoto (2008), Frictional melt and seismic slip, *J. Geophys. Res.*, *113*, B01308, doi:10.1029/2007JB005122.

Nielsen, S., P. Mosca, G. Giberti, G. Di Toro, T. Hirose, and T. Shimamoto (2010), On the transient behavior of frictional melt during seismic slip, *J. Geophys. Res.*, *115*, B10301, doi:10.1029/2009JB007020.

Niemeijer, A., G. Di Toro, S. Nielsen, and F. Di Felice (2011), Frictional melting of gabbro under extreme experimental conditions of normal stress, acceleration and sliding velocity, *J. Geophys. Res.*, *116*, B07404, doi:10.1029/2010JB008181.

Noda, H., E. M. Dunham, and J. R. Rice (2009), Earthquake ruptures with thermal weakening and the operation of major faults at low overall stress levels, *J. Geophys. Res.*, *114*, B07302, doi:10.1029/2008JB006143.

Palmer, A., and J. Rice (1973), The growth of slip surfaces in the progressive failure of over-consolidated clay, *Proc. R. Soc.*, *332*, 527–548.

Peyrat, S., K. B. Olsen, and R. Madariaga (2004), Which dynamic rupture parameters can be estimated from strong ground motion and geodetic data?, *Pure Appl. Geophys.*, *161*, 2155–2169.

Poliakov, A. N. B. (2002), Dynamic shear rupture interactions with fault bends and off-axis secondary faulting, *J. Geophys. Res.*, *107*(B11), 2295, doi:10.1029/2001JB000572.

Rice, J. R. (2006), Heating and weakening of faults during earthquake slip, *J. Geophys. Res.*, *111*, B05311, doi:10.1029/2005JB004006.

Shipton, Z. K., J. P. Evans, R. E. Abercrombie, and E. E. Brodsky (2006), The missing sinks: Slip localization in faults, damage zones, and the seismic energy budget, in *Earthquakes: Radiated Energy and the Physics of Faulting: American Geophysical Union, Geophys. Monogr. Ser.*, vol. 170, pp. 217–222, AGU, Washington, D. C.

Smith, S., S. Nielsen, and G. Di Toro (2015), Strain localization and the onset of dynamic weakening in calcite fault gouge, *Earth Planet. Sci. Lett.*, *413*, 25–36, doi:10.1016/j.epsl.2014.12.043.

Tinti, E., P. Spudich, and M. Cocco (2005), Earthquake fracture energy inferred from kinematic rupture models on extended faults, *J. Geophys. Res.*, *110*, B12303, doi:10.1029/2005JB003644.

Viesca, R. C., and D. I. Garagash (2015), Ubiquitous weakening of faults due to thermal pressurization, *Nat. Geosci.*, *8*, 875–879, doi:10.1038/ngeo2554.

Violay, M., G. Di Toro, B. Gibert, S. Nielsen, E. Spagnuolo, P. Del Gaudio, P. Azais, and P. G. Scarlato (2014), Effect of glass on the frictional behavior of basalts at seismic slip rates, *Geophys. Res. Lett.*, *41*(2), 348–355, doi:10.1002/2013GL058601.

Violay, M., G. Di Toro, S. Nielsen, E. Spagnuolo, and J. Burg (2015), Thermo-mechanical pressurization of experimental faults in cohesive rocks during seismic slip, *Earth Planet. Sci. Lett.*, *429*, 1–10, doi:10.1016/j.epsl.2015.07.054.